RC: 1. General comments.

The authors have improved the manuscript and addressed main concerns of the two reviewers. The formulations were chosen to be less generalized and more specific to the investigated avalanches and the friction calculation is now more reasonable and understandable. The differences of energy sources between friction and entrainment is now supported by an additional calculation of entrainment.

However, other points are not considered, which I will list below. There is still a problem that presented data is not able to support a conclusion. The main problem is the insufficient description of the used methods.

I disagree with the assumption that the IRT camera is a useful tool for qualitative comparisons for temperatures after an avalanche stopped. The presented verification and existing literature does not allow this statement. This requires more careful formulations.

AC: We thank the reviewer for the high quality of this review and for his/her constructive comments. We think the reviewer is right that there were parts in the manuscript, which did not allow to completely follow the applied methods and data processing and thus the link to the conclusions was not sufficiently supported. Now we added all information requested, in particular the details on the lateral temperature profiles, the avalanche mass balance calculations and the presented (basic) verification of the IRT data with field measurements.

Overall, we still consider the IRT camera as a useful tool for qualitative interpretation, but we acknowledge that there are many points, which are not understood yet. The authors believe that the controversial discussion on the application of IRT highlights the importance of further investigations as well as the discussion in this manuscript.

The results only contain data on the IRT measurements which could be clearly verified with other observations, such as powder cloud behaviour (Section 4.1.1.) and surface temperature distributions in Section 4.1.2. All other interpretations of the IRT data are contained in the discussion and are marked as hypothetical. There we also discuss our basic verification and additional literature. Already in the abstract we noted that we want to “discuss” the application of IRT in the field of avalanche dynamics. We stated multiple times that based on the work in our study, further verification is needed to elaborate the potential of IRT in this field, which is, as the authors believe, significant.

We are aware that our dataset contains a limited amount of avalanches (which is rather common for field observations of real-scale avalanches) and general conclusions cannot be drawn. We therefore re-worded our conclusions to be only valid for the investigated avalanches and structured our discussion in such a way that it provides suggestions for future work in this direction. We would like to note that the presented dataset (consisting of multiple snow profiles, laser scanning data for mass balance calculations and supplemented with IRT data) is the most comprehensive one available when it comes to thermal investigations in the field of avalanche dynamics. The effort in collecting this data set was substantial and it will be a very valuable data set for model verification in future.

In the following, we will answer the reviewers’ specific questions in detail.

2. Specific comments

2.1 Conclusions are not supported by the data

RC.1: The main conclusion is that friction was the main energy source, which was dependent on the drop height. This is solid after discussing Figure 9 and Table 2. The authors should only be more precise that it is in fact dependent on the effective drop height, which is dependent on the growth index (Eq 3).
AC.1: We now emphasize this in more detail in the manuscript.

RC.2: However, the conclusion that entrainment varied between the avalanches does not hold, because of insufficient analysis and presentation of the data.
AC.2: We describe the calculation of the mass balance (Section 2.5) for avalanche #2 and #3 in more detail to illustrate how we analysed the data. Also see AC.10 for a detailed description.

RC.3: The authors presented warming due to entrainment of 0.08 and 0.3 degrees. The calculation is very questionable. Firstly, it is not clear to me how the temperature difference between mass released and mass entrained is calculated, which was used in Eq. 4. I can only assume it is the difference of T_Prelease and T_Ptrack, averaged over the solid lines shown in Figure 9, with excluding the grey areas.
AC.3: Yes, the reviewer is correct that the temperature difference is the difference between the (depth-averaged) entrained (T_Ptrack) and released snow (T_Prelease). We clarified Eq. 4 by explicitly writing T_Ptrack and T_Prelease instead of introducing a new variable for this temperature difference (deltaT_rel-ent). This formulation of Eq. 4 also directly results in the, now corrected, values of the temperature change due to entrainment. This is typically a warming (as shown for avalanche #3 with 0.3°C) but can also result in a (slight) cooling (avalanche #2 with -0.08°C) depending on the entrainment depth and the corresponding snow temperatures.

In addition, we also clarify now in the manuscript that the grey areas were only excluded for the profiles in the centre of the deposition zone (P_depo). For the other profiles in the undisturbed snow cover (P_release, P_track) no significant influence was expected in the relatively short amount of time between release and the measurements. We are sorry if we did not formulate this clearly in the previous version.

For the measurement procedure we want to add: The temperature of the release has been directly measured in the release zone after the avalanche around 0.5 m behind the fracture line. The part of the snowcover, which released is represented by the continuous line in Figure 9 (h_rel=1.03 as written in brackets in Table 2), while the part of the snow cover, which has remained in place, is represented by the dotted line. The release temperature shown in Table 2 is the average of this continuous blue line. The same was conducted for the temperature of the entrained mass (continuous orange line). This temperature corresponds to the average temperature of the entrained snow along the path.

RC.4: Besides this ambiguity it is concerning that that these plotted results do not correspond to the calculated values in Table 2, to my opinion. I see a positive difference between the blue and the orange temperature profile in average for both cases, maybe even a larger one for avalanche #2 (left). In Table 2 this impression is not represented. A smaller (and negative!) change was mentioned for avalanche #1. This is directly affecting the conclusion “varied between avalanches”.
AC.4: We agree that averaging the temperature profiles (solid lines) “by eye” gives this impression and is irritating when comparing to the values in Table 2. Yet, calculating the average for the solid lines results in the presented numbers. Additionally-Figure A shows the averaged values (as presented in Table 2) as vertical lines.

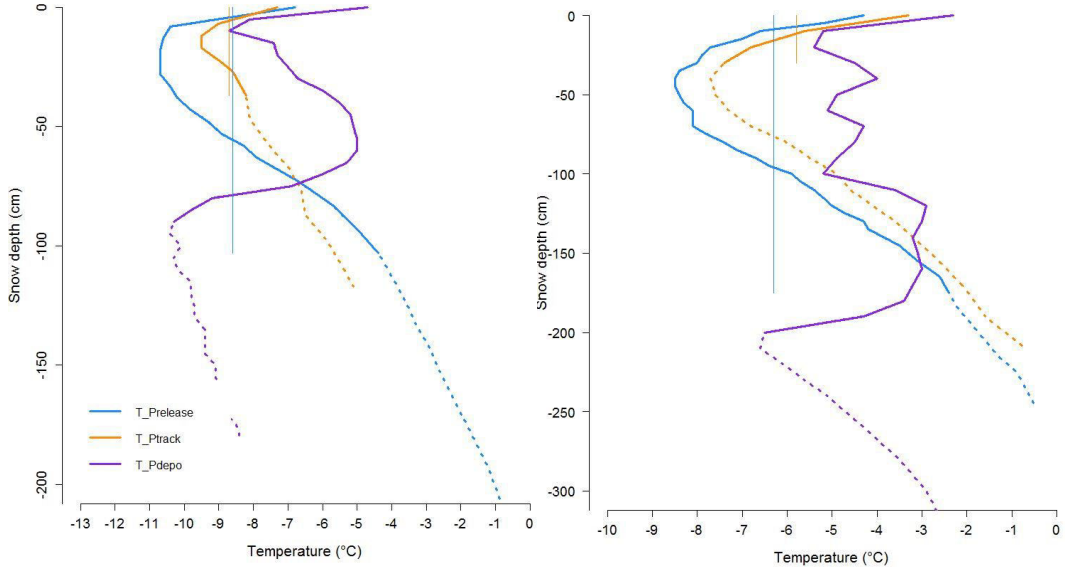

Additional-Figure A: Simplified illustration of Figure 9 in the manuscript. Colored vertical lines indicate the averaged values (Table 2) of the corresponding solid lines.

Therefore, the statement that there was a difference in temperature between released and entrained snow and also between the investigated avalanches persists. Furthermore, generally speaking, one can imagine the possible range of different temperatures with varying release and/or entrainment depths for other avalanches (as mentioned in the discussion section of the manuscript).

RC.5: The fact that Table 2 states that T_Ptrack is 0.1 degree cooler in average compared to T_Prelease is very concerning. A warming due to entrainment cannot be explained with Eq. 4, as the authors stated, it would result in a cooling. The authors need to be clearer that they do not make two mistakes here, firstly wrong averaging, secondly, a sign error.
AC.5: The reviewer is correct that a minus sign was missing for avalanche #2 (DTentrainment = -0.08°C) in this calculation and consequently in Table 2. We corrected this in the manuscript. As presented in AC.4, the averaging for the temperature profiles is correct.

Generally speaking and only focusing on temperature changes due to entrainment an avalanche can also cool if the avalanche released into deep layers (recall in the snowcover temperature increases with depth and typically reach 0°C) but entrains only superficial layers of snow, which can be the coldest (e.g. blue and orange lines in Figure 9).

RC.6: In the discussion section the authors stated that deposits from powder cloud has consistently lower temperatures than the warm dense core (line 615ff). It is not clear to me if the author refer to the general impression of IRT images or to Figure 7, where the authors presented lower temperatures for two transects out of 4, which show lower temperatures for a thin deposition area. This is one example of how the reader does not know exactly how the authors argue and leave the reader unsure (see section 2.2 below for other examples). For both interpretations I have concerns. For the IRT images my opinion is that also qualitative relations may not be possible and therefore the authors may not be able to state this conclusion (see comments to IRT images in section 2.3).
AC.6: We aimed to refer to the IRT data acquired with videos (and the corresponding screenshots in Figure 3 and 5) and not to Figure 7. We updated the manuscript with an explicit reference to the specified data. Generally, we agree with the reviewer that this is only a qualitative observation which needs to be treated carefully in the paper. Therefore, we did not state this observation as a conclusion but added it in the discussion section. However, these observations are supported by other research (Sovilla et al, 2015) which shows that, at the nose, powder avalanches tend to entrain a thin layer of superficial cold snow where the cloud develops. The measurements of Flüela confirm this tendency.

RC.7: For the lower temperatures in the thin deposits compared to the dense core in Figure 7 (transect L1 and L2), I am unsure by the presented material if these transects are indeed covering deposits in the middle of the avalanche, where the authors assume deposits of the dense core. Comparing Figure 6b, showing the transects, and Figure 1b, showing visual photo of the avalanche, I would assume especially for L1 that this transect covered an erosion zone in the middle of the avalanche (while at the side L1 is indeed covering thin deposition). The higher temperatures in the middle of the avalanche could be those of the exposed warmer bed surface of the avalanche (warmer temperatures are deeper in the snowpack).

AC.7: We appreciate the very detailed interpretation of our results by the reviewer. Additionally Figure B below shows a panoramic picture of avalanche #2 (mind the photographic distortion as it is a composite of multiple pictures!) which was taken in the centre of the avalanche path looking down slope. The large blocks of snow can also be identified in Figure 1b in the centre of the avalanche where the deposition starts and corresponds approximately to an altitude of L1 in Figure 6b. Looking at the right side of the picture it becomes evident that this area is covered with debris and does not expose the sliding surface / erosion area. We also noted this now in the updated manuscript.

The fact that the temperature of the dense core in Figure 7 are similar in L1 and L2 (approximately -6.3°C) and L3 and L4 (approximately -6.5°C) suggests that the temperature of the deposit of the dense core is rather constant along the path suggesting a good mixing of the snow.

Additional-figure B: Deposition are of avalanche #2.

RC.8: Another observation makes me thinking that rather erosion areas were analysed in L1 and L2. Figure 1b shows that also at L3 and L4 there are areas of thin deposition at the sides of the transects. Why aren't there differences in temperatures for those transects? I assume, because L3 and L4 covered deposition, while L1 and L2 covered erosion in the middle of the avalanche?

AC.8: We cannot disagree with the reviewer that a narrow part of the outer sides of transects L3 and L4 possibly belongs to a thin deposition area. Yet, neither the IRT signal (the thin deposit area might be "hidden" in the increasing temperatures towards the dense core between approximately 5-15 m lateral distance in Figure 7c) nor investigations in the deposits (Figure 1b and Additional-figure B) allow a clear separation as for areas such as L1 and L2. Also keep in mind that Figure 1b and the IRT measurements in Figure 6b were not taken from the same position. Therefore L3 and L4 are in the very lower part (nearly flat part) of Figure 1b.

RC.9: Please ensure the reader that not an erosion zone was analysed in L1 and L2 in Figure 7. This makes the conclusion in lines 615ff problematic that deposits from the powder cloud has consistently lower temperatures than the warm dense core, as well as the statement in lines 600ff that the IRT can be used to "…could be the differentiation of flow regimes in the deposition area".

We try now to eliminate the doubt of the reader by better specifying where the deposition zones are visible. See AC.7 for further details. Furthermore, as mentioned in AC.6 we now clarified the statement related to the lower temperatures of the powder clouds and that we did not refer to Figure 7.

Nevertheless, field investigations show that the deposits are characterized by different regions, normally identifiable by different characteristics of the superficial texture. In avalanche dynamics, we attribute these differences to the different flow regimes, distinguishing between dense/dilute-fluidized-energetic/powder. This is common practice (Isller et al, 2008; Gauer et al, 2008, Bartelt et al, 2012) These differences can be seen with the IRT camera. Yet, with our analysis we cannot conclude that the absolute differences in temperatures are real because the surfaces have different roughness and thus, can influence the measurements. Nevertheless, the differences are clearly visible, independently where they are coming from, and this is all what we want to show.
We do not disagree with the reviewer that it is an open question if this is valid as a general statement and can be observed for other avalanches. For this reason we formulated this part in the discussion as a "possible further application of IRT".

2.2 Description of methods

RC.10: It is still unclear to me (although requested by reviewer #2) how the released and entrained mass was determined, both for avalanche #3, for which the TLS scans are completely available, and for avalanche #2 with incomplete TLS scans. This is quite important since it is affecting the conclusion "entrainment energy varied between avalanches" (Eq. 4). Please add a description how the area of release vs. entrainment was determined. This area was maybe then used to calculate mass with depth and density from profiles and TLS data? The reader is forced to guess here. Please also add how the "averaged density" of the release and entrainment was determined. I assume with profiles and it is reasonable to assume which profiles, but I think this information could be added for more clarity. For avalanche #2 the scan before the avalanche is missing partly. The authors stated that the erosion was quite homogeneous, that's why they could extrapolate to the missing parts. This would also include the assumption that the surface before the avalanche was quite homogeneous, since the scan before the avalanche is missing. Please discuss that there were for example no larger drifts present, or other rough areas. How was the extrapolation done afterwards? With the perimeter of the avalanche determined with GPS measurements? Please be a bit more precise here.
AC.10: As requested a more detailed formulation of the mass balance calculation was added to Section 2.5 including references to literature where this procedure was applied.

For avalanche #3 a TLS was available before and after the artificial release of the avalanche. This allowed to define the areas of release, entrainment and deposition and to calculate their spatial extents. The difference between the TLS before and afterwards facilitated the calculation of a spatially averaged release/entrainment depth. Note that these average depths might not correspond to the local depths acquired in the snow profiles (i.e. Table 2). As snow profiles were available for the release (P_release) and along the avalanche path (P_track) the (vertically averaged) snow density could be calculated. This allowed to separately calculate the released and entrained mass which in total results in the deposited mass. The resulting values for the deposited mass were cross checked by calculating the mass from the deposition area and the snow depth and density from the profile in the centre of the deposits.

For avalanche #2 the TLS before the event is incomplete, only consisting of the release and parts of the erosion area. The scan after the avalanche (and also the GPS measurements) allowed to clearly delineate the envelope of avalanche #2 and again the release, entrainment and deposition areas were identified and calculated. As the erosion along the path was rather homogenous (Figure 1b), we could assume the same erosion depth for the lower part (i.e. were no TLS measurements are available) as for the upper part of the erosion area (see Figure 2) and consequently apply the same procedure as for avalanche #3. As can be seen in Figure 1b no larger wind drift events were present and the surface is generally rather "smooth" along the slope below the rock face and the runout area.

RC.11: Both reviewer wanted more information on the BTS measurements, which was not added as the comments suggested. BTS measurements were interpolated for Figure 8. I know now that they took 3-5 min, but I am unsure if it is for one location with several measurements in depth, or indeed for one single temperature measurement. 3-5 min for the latter is certainly long enough. If the authors would have done 10 measurements in 3 min at different depth, I would be worried if the not mentioned Time Constant for the thermocouples was met. Please be clearer here and also provide information of the vertical resolution.

AC.11: Each measure took 3-5 minutes and the measurements were performed with two probes. Measurements started simultaneously from right and left of the deposit toward the centre of the deposit. At the same time the snow profile in the centre of the deposits (P_depo) was conducted. We added the total time (1-2 hours) in the (last) reviewer answers but now added it also to the manuscript to avoid confusion. Vertically, the measurements were conducted in steps of typically 30 cm. All this information was now added to the manuscript.

RC.12: Please provide information on the horizontal resolution of the regular spaced pits which were used to determine the depth of the deposits.

AC.12: For avalanche #2 a full trench (see Additional-Figure C) was dug where the measurements were performed. While a team was conducting the excavation other persons conducted the snow profiles, especially the temperature measurements, immediately afterwards. Horizontal resolution is given in Figure 8 as location distance (m) away from the centre profile (P_depo). For avalanche #3 localized pits were dug at selected locations of the BTS probe measurements to determine the deposition depth in addition to the snow profile in the centre (P_depo).

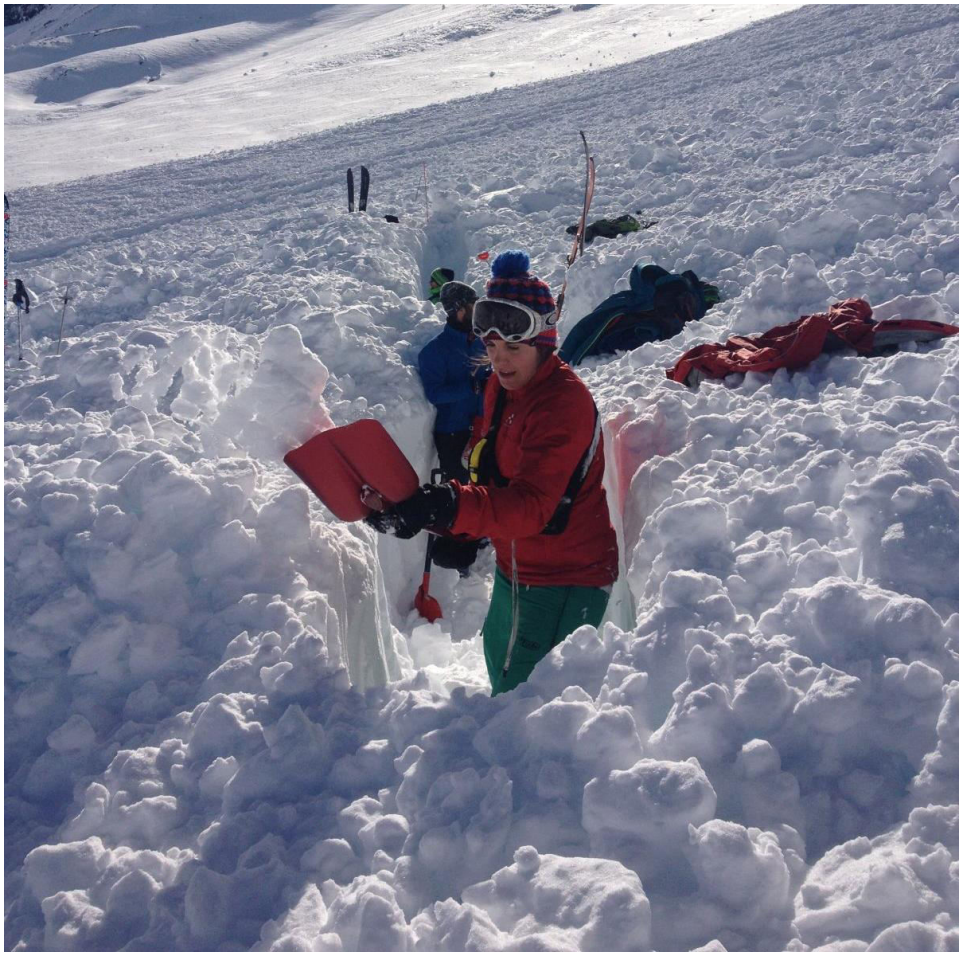

Additional-figure C: Excavation of the measurement trench for avalanche #2.

RC.13: Figure 8: It is not clear to me how the solid line showing the surface of the avalanche deposits, as well as the surface of the ground (dotted) was determined. With a combination of GPS measurements of the transect and TLS measurements?
AC.13: The distance from the top (solid line) to the bottom (dashed) of the deposit resulted in the depth of the deposit (see also question above). As the surface of an avalanche deposit (with its highest point usually in the centre) is not flat, data from the TLS and the summer DEM combined with GPS coordinates of the measurement locations allowed to define the absolute height of the deposits resulting in Figure 8 with the lateral location distance 0 (corresponding to the location of P_depo) in the centre.

RC.14: The caption and the text for Figure 4 is confusing. I am unsure what was measured at the surface and what at the corresponding layer in the profile.
AC.14: We agree with the reviewer that the caption of Figure 4 and the corresponding text was not formulated clear enough. This was now adapted in the manuscript.

RC.15: The authors state in the text that the surface temperature was measured "along the erosion layer" in the avalanche path at P_track (line 192f), which I would interpret as the temperature of the bed surface of the avalanche. However, the grey colour in Figure 4, as well as the figure caption, that T_P_track was related to the surface of undisturbed snow next to the avalanche. Please be clearer here.
AC.15: The reviewer is right that this was misleading information. We now corrected this and formulated it better in Section 2.4 as well as in the caption of Figure 4. Also see AC.14.

RC.16: Also, why was not the corresponding layer temperature (not surface temperature) compared with the IRT of the bed surface at time 0 min similar to T_P_release? And why did the authors not include avalanche #3 in the verification? If there are no surface temperatures available, the authors have data from the profiles and the corresponding layers at the release and along the track for time 0 min.
AC.16: We now added and described the measurement of the snow profile along the track,T_Ptrack, to Figure 4. Also see AC.14. Avalanche 3 was released during very stormy conditions (see Additional-Figure D). Even though IRT images were acquired during the avalanche with 30 Hz and afterwards combined with visual images in timesteps of one minute, this data set could not be used in this study as clouds were mostly preventing an undisturbed view on the slope.

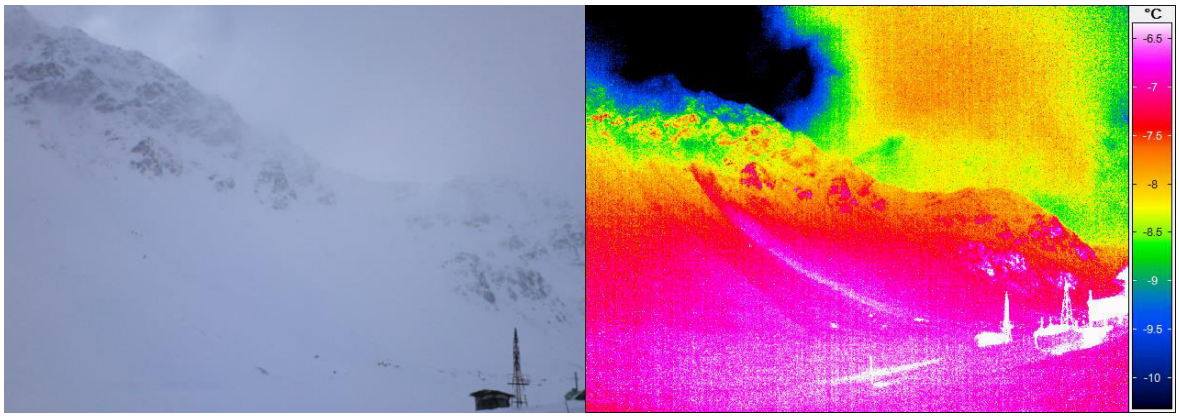

Additional-Figure D: Example data acquired with the newer IRT camera setup for avalanche #3. The visual image (left) and an IRT image (right) illustrate the challenging conditions during this field experiment as clouds continuously moved between the slope and the IRT camera. Even though the persons in the visual image could still be identified in the IRT image, the IRT data could not be used for further, quantitative, analysis.

RC.17: In Figure 4 the IRT data is presented as continuous lines. What was the temporal resolution of taking pictures? I assume no video was made during one hour.

AC.17: The presented lines are interpolations between measurement points. IRT pictures were manually taken at regular intervals. We describe this now in the caption of Figure 4 and also added markers, which visually represent the temporal resolution to one of the lines (IRT_track_undisturbed, orange dashed).

Note that the newer camera model allowed acquiring IRT and visual images simultaneously with a temporal resolution of one minute. This would allow for a much more continuous data series. (See AC.16)

RC.18: Please mention in the methods section for what the summer DEM data is used. Right now the summer DEM is in section 2.5 TLS, while in fact it is only used for IRT, to georeferenced the images and calculate the mass of the avalanches. Please also mention the source of the summer DEM.
As suggested by the reviewer we added this information to the methods section. The used summer DEM was acquired during an airborne digital photogrammetry campaign (Buehler, 2015). In our study we did not use the summer DEM for mass balance calculations as described in Section 2.5. It has been used to calculate the release mass based on IRT and snow profile data to test a new possible methodology. This use is shortly discussed in the discussion section, Further, is has been used to georeference our data for processing in a GIS System.

RC.19: In Figure 6 the IRT pixels of the transects were related to real distance using the width of the avalanche. I suggest to have pixel number on the x-axis and rather indicate for the width of the avalanche in the Figure, since there is obviously no clear relationship between pixel size and real distance.
AC.19: There is the possibility to simply scale the pixel distance to the real distance. In our opinion it is better to have a reference to the real distance, even if it only has a relatively coarse accuracy rather than having a pixel distance which cannot be compared to other measurements. We will leave the graphic with the real distance and add in the manuscript that the width was scaled to measurements.

RC.20: There are some rounding issues using Eq. 2 and 3. I calculate 1.39 instead of 1.5 (line 435), and 0.96 instead of 0.9 (line 454).
AC.20: In an initial calculation we rounded the initial parameters (g=10 m / s2 instead of 9.81 m / s2 and cp = 2000 J / kg / K instead of 2116 J / kg / K) which resulted in 1.5°C instead of 1.39°C and consequently 0.9°C instead of 0.96°C. The values have been accordingly corrected.

2.3 Qualitative interpretation of IRT images

RC.21: To my opinion the authors should be more careful with the qualitative interpretation of the IRT images. In the introduction the authors concluded based on their literature review that IRT can be seen as a useful qualitative tool for snow applications (line 86ff). But the before cited study of Schirmer and Jamieson showed the opposite. After only some seconds (!) they found relative warm areas in an exposed snow profile which were quite probably not warmer in the unexposed snowpack, with increasing relative differences in the next few minutes. This means that relative differences are not possible in such a scenario of exposing snow to a new environment.
AC.21: The scale of the processes looked by Schirmer and Jamieson, i.e. a single roughness element, is different than from the scale we were looking at in our investigations. A first approximate analysis shows that, for example, the detail of the release in the infrared camera showed warmer temperature were the snow released deeper. This information from the IRT camera is perfectly in agreement with information from laserscannig and manual profiles. Thus, one needs to be careful to state that the camera cannot give good qualitative results on other scales and situations than investigated by Schirmer and Jamieson. In fact, a more detailed validation is currently carried out at our institute (Personal communication). We agree with the reviewer that the temperature oscillations around the mean that we can see in Figure 7 may be an effect of the phenomenon described in Schirmer and Jamieson.

RC.22: I would assume that an avalanche with warm particles in motion exposed to cold air may act in a very similar way as exposing a snow profile. In both cases the area of interest is certainly not in a

thermal equilibrium with the surrounding atmosphere. This is also the main difference to cirrus clouds, which the authors refer to as a similar example, for which IRT is successfully used (line 596ff). I would suggest to change this formulation here in line 86ff, since I would say this cannot be concluded with cited literature.
AC.22: As suggested by the reviewer we rephrased the formulation in the introduction. We also agree with the reviewer that an avalanche (both powder cloud and exposed dense core) are definitely not in thermal equilibrium with its surroundings. As noted in the discussion, the comparison to cirrus clouds was intended to relate to tracer applications, i.e. purely at the qualitative level. In general, I would not state that cirrus clouds are in thermal equilibrium with its surroundings. Even though they consist of ice particles and are moving at very high altitudes they will rarely be in exact thermal equilibrium with the surrounding atmosphere for longer periods of time. Hence, we expect similar challenges in the field of airborne or satellite remote sensing and see the cited literature as motivation for further (snow related) studies.

RC.23: In Figure 7 thin deposits have slight differences in temperatures (<1 degree) compared to deposits from the dense core (see also my comment above that I am unsure if there were really deposits covered by transects L1 and L2 in the middle of the avalanche). This is a qualitative usage, and I have a strong concern with this qualitative usage. Visible by eye in Figure 1b is that there was certainly a difference in surface roughness between the two areas. If this was the main reason why the IRT images showed differences, then I do not see a benefit to a visual picture. There needs to be some more investigations that there is more value in an IRT image compared to a visual image for distinguishing deposition areas.
AC.23: The distinction between areas of different flow regimes and deposition zones in the field is not trivial at all and always subject to speculations. Further, there are very few occasions where, after an avalanche, there is the possibility to access the deposition zone for manual measurements. Thus, there is a general need to methods to clearly distinguish, in the deposits, but also along the path, areas belonging to different flow processes. In our case the IRT signals supported our visual observations. However, it is also clear that to allow for more quantitative conclusion more research needs to be performed. In particular, it is not clear which flow regimes can be identified in the field, and the influence of roughness elements at widely varying scales on the IRT signal. Both questions are out of scope of this manuscript. Yet, we aimed to illustrate and discuss that observed differences in the IRT measurements corresponded to different areas in the avalanche deposits. Which is of significant relevance for the application IRT in the field of avalanche dynamics (and other snow science disciplines).

RC.24: The IRT images were taken less than one minute after the avalanche stopped (line 167). The cooling speeds shown in Figure 4 are on a much longer time scale (several minutes to up to one hour). This is why I do not like the authors' reply. I am interested in a much shorter time scale to trust Figure 7, which is the time between the deposition and the time of the image used for Figure 7. The authors correctly argued that the coarse resolution may not result in similar problems as in Schirmer and Jamieson (2014). The authors argued that over a footprint of 1 m there may be a more isotropic signal character. However, this is only a hypothesis, which can be easily tested with the existing data the authors have. One can argue using their argument, that there is a qualitative difference based on the small scale roughness how much more isotropic the signal character is. This is why there should be more done with existing data. As I understand, the authors made IRT videos of the moving avalanche, eventually stopped the videos and took pictures. So there is data available leading to the data shown in Figure 7 which can be analysed on different cooling speed based on roughness differences. No laboratory experiments are needed for this investigation.
AC.24: Yes, the time scale in Figure 7 is much longer than the initial cooling that takes place. The only data we have to investigate the time scales requested by the reviewer are the videos acquired during the avalanche release and directly after they stopped (see supplementary material). A cooling of the dense core area can be well observed in the video of avalanche #1. After the powder cloud drifts aside the dense core seems to cool (between timesteps 0:17 and 0:22). Yet, we obviously could not verify this with any other measurement. As this is hardly possible in real scale experiments we propose creating large samples (larger than the ones in Schirmer and Jamieson (2014)) of varying

roughness, warming them in laboratory environment and then exposing them to different environmental conditions.

For our investigation we have to make the assumption that from the time the avalanche stopped until the first measurement less than a minute later, i.e. timestep 0 in Figure 7, the different surface roughness of different areas in the deposits exhibits a similar temperature change rate.

Manuscript prepared for J. Name
with version 2014/05/22 6.83 Copernicus papers of the LaTeX class copernicus.cls.
Date: 17 July 2015

Thermal energy in dry snow avalanches

Walter Steinkogler[1,2], **Betty Sovilla**[1], **and Michael Lehning**[1,2]

[1]WSL Institute for Snow and Avalanche Research SLF, Davos Dorf, Switzerland
[2]CRYOS, School of Architecture, Civil and Environmental Engineering, EPFL, Lausanne, Switzerland

Correspondence to: Walter Steinkogler (steinkogler@slf.ch)

Abstract. Avalanches can exhibit many different flow regimes from powder clouds to slush flows. Flow regimes are largely controlled by the properties of the snow released and entrained along the path. Recent investigations showed the temperature of the moving snow to be one of the most important factors controlling the mobility of the flow. The temperature of an avalanche is determined by the temperature of the released and entrained snow but also increases by frictional processes with time. For three artificially released avalanches, we conducted snow profiles along the avalanche track and in the deposition area, which allowed quantifying the temperature of the eroded snow layers. This data set allowed to calculate the thermal balance, from release to deposition, and to discuss the magnitudes of different sources of thermal energy of the avalanches. For the investigated dry avalanches, the thermal energy increase due to friction was mainly depending on the effective elevation drop of the mass of the avalanche with a warming of approximately 0.3C per 100 height meters. Contrary, ~~warming~~ the temperature change due to entrainment varied for the individual avalanches, from ~~0.08~~ -0.08 to 0.3C, and depended on the temperature of the snow along the path and the erosion depth. Infrared radiation thermography (IRT) was used to assess the surface temperature before, during and just after the avalanche with high spatial resolution. This data set allowed to identify the warmest temperatures to be located in the deposits of the dense core. Future research directions, especially for the application of IRT, in the field of thermal investigations in avalanche dynamics are discussed.

1 Introduction

Avalanches can exhibit many different flow regimes (Gauer et al., 2008) depending on 1) the released and entrained amount of snow, 2) the properties of the snow and 3) the topography (slope, curvature) (Naaim et al., 2013). Studies showed that avalanches can increase their mass due to entrainment by multiple factors (Sovilla et al., 2007; Bates et al., 2014) which in turn influences the run-out distance. Even though important, the amount of snow entrained is not the main controlling factor that determines the flow form of the avalanche (Bartelt et al., 2012). The flow regimes and in turn mobility are strongly influenced by the properties of the entrained snow (Steinkogler et al., 2014b). Data on front velocities, run out, flow regimes and powder clouds revealed that different avalanches can form with similar release conditions and on the same avalanche path depending on the inherent snow cover properties. Advancements in avalanche dynamics models allow to account for the properties of the flowing snow with more and more detail (Vera Valero et al., 2015).

Recently, it has been shown that snow temperature inside an avalanche can significantly change its flow dynamics (Naaim et al., 2013; Steinkogler et al., 2014b), mainly by changing the granular structure of the flow (Steinkogler et al., 2014a). Laboratory studies on the granulation of snow showed a distinct dependency on snow temperatures with a fundamental change in snow structure at a threshold of -1C. Therefore, significant changes in flow dynamics can be expected with relatively small changes in temperature around this threshold.

Measuring temperature inside a flowing avalanche or in its deposit with traditional methods has proven to be difficult due to technical constraints or because measurements can not be conducted due to safety reasons. In addition to manual snow profiles we therefore investigate the application potential of infrared radiation thermography (IRT) technologies. IRT is a non-contact, non-intrusive technique, which enables us to see surface temperature in a visible image. Meola and Carlomagno (2004) give an overview on existing work and describe the most relevant industrial and research applications of IRT.

The emissivity of a surface is a function of many factors, including water content, chemical composition, structure and roughness (Snyder et al., 1998) as well as the viewing angle between observer and measurement object. Even though many technical challenges and shortcomings of IRT are known, possible applications on the field of snow science have recently been discussed (Shea and Jamieson, 2011). Shea et al. (2012) and Schirmer and Jamieson (2014) applied IRT to measure spatial snow surface temperatures on snow pit walls. It was found that fast and large temperature changes resulting from surface energy balance processes must be expected (Schirmer and Jamieson, 2014). These energy balance processes between air and snow are particularly important during windy conditions, clear skies and large temperature differences between air and snow. These findings indicate that measuring the snow surface temperature of avalanche deposits or erosion layers along the track must be carried out as fast as possible. If IRT can therefore be seen as a useful qualitative or quantitative tool for snow applications ~~whose quantitative operation~~ still needs further verification.

The aim of this study is to identify the spatial temperature distribution in an avalanche and to quantify potential sources of thermal energy in an order of magnitude estimation. This is achieved by field measurements and the application of an IRT camera. A secondary aim is to evaluate the application of the IRT technique to get deeper insights into the thermal state of an avalanche.

2 Methods & Data

2.1 The Flueelapass field site

Multiple dry avalanches were artificially released during winters 2012-13 and 2013-14 at the Flueelapass field site above Davos (Switzerland). Here we will discuss three avalanches, #1 (23 January 2013), #2 (05 February 2013) and #3 (31 January 2014), out of this data base (Fig. 1).

The avalanche path is a north-east facing slope covering 600 vertical meters. Deposits of larger avalanches typically reach a lake located at 2374 m a.s.l. at the bottom of the slope (Fig. 2). Observations and remote measurements can safely be conducted from the road at the pass which is approximately 800 m away from the avalanche. The slope angle ranges from 50 in the rock face in the upper part to 20 at the beginning of the run-out zone with an average of 30 of the open slope around 2600 m a.s.l..

2.2 Snow profiles

To assess the properties of the released and entrained snow, manual snow profiles according to Fierz et al. (2009) were conducted in the release zone ($P_{release}$), i.e. just below the rock face, along the track (P_{track}), in the deposition zone (P_{depo}) and in the undisturbed snow cover in the run out zone (P_{runout}) (Fig. 2). The profile location of the initially released cornice is refereed to as $P_{cornice}$. In combination with release and erosion depths, the acquired snow profiles allowed to identify which layers were entrained into the avalanche.

All profiles were conducted as fast as possible after the avalanche stopped. Yet, especially for the profiles in the release area and the track, it took around 30 minutes to reach the profile locations. The temperature measurements close to the surface must therefore be interpreted carefully due to a rapid adaptation to the ambient conditions.

In addition to the acquired video and pictures of the powder cloud the deposits of the avalanche were investigated for indications of different flow regimes according to the observation criteria of Issler et al. (2008).

2.3 Lateral temperature profiles

In addition to the regular snow profiles, trenches were dug in the deposition zone and modified avalanche probes were used to measure lateral temperature gradients. The modified temperature probes (BTS probes) are regular avalanche probes for which the tip was replaced by a thermistor. BTS probes are usually used for permafrost applications (Lewkowicz and Ednie, 2004; Brenning et al., 2005) to measure the temperature at the interface between soil and snow. Their application allowed to measure the temperature of snow layers without exposing them to the ambient air temperature. As for the thermometers used for regular snow profiles (Section 2.2) they measure the snow temperature with an accuracy of $\pm 0.1°C$. As for the regular snow profiles the upper most layers need to be interpreted carefully in this investigation due to an expected change in temperature over time. The lateral temperature measurements were conducted ~~to~~ from the left and right side ~~of~~ towards the snow profile P_{depo}, which was situated in the center of the deposition zone (Fig. 2). ~~Every BTS~~, simultaneously. The BTS probe measurements were conducted with a vertical resolution of typically 30 cm and each individual measurement took around 3-5 minutes. ~~The interface between deposits and the undisturbed snow cover underneath could be identified in a rapid gradient in the temperature measurements. The~~, giving the thermistor sufficient time to adapt to the snow temperature. In total these measurements took 1-2 hours. Additionally, the snow depth of the deposits was determined by regularly spaced pits along the transect after the temperature measurements ~~.~~ for avalanche #3. For avalanche #2 a full trench was dug were the measurements were performed.

2.4 Infrared radiation thermography (IRT) camera

The snow temperature measurements acquired from profiles where supplemented with an infrared radiation thermography (IRT) camera which allowed to record snow surface temperatures before, during and after the avalanche (Fig. 3 and 5). Time-lapse measurements after the avalanche stopped al-

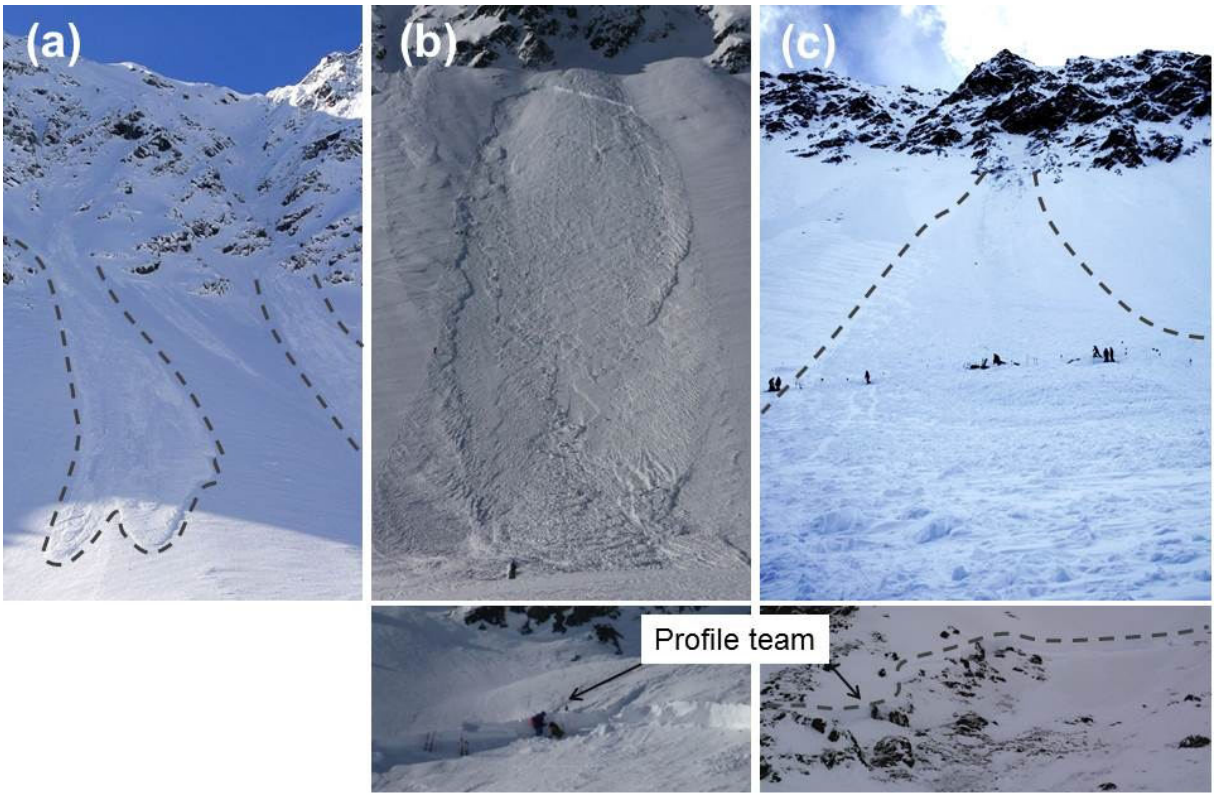

Figure 1. Avalanches at the Flueelapass field site released by artificial triggering of the cornices on the ridge. Avalanche #1a and #1b (a) were released on 23 January 2013, #2 (b) on 05 February 2013 and #3 (c) on 31 January 2014. Note the significant secondary release and entrainment of deeper layers below the rock face for (b) avalanche #2 and (c) avalanche #3.

lowed to follow the temporal evolution of surface temperatures (Fig. 4) and videos of the moving avalanche provided a qualitative yet illustrative point of view (provided as supplementary material). The first pictures were recorded as fast as possible (usually less than 1 minute) after the powder cloud disappeared and the video recording was stopped.

We used an InfraTec VarioCAM hr 384 sl and a VarioCAM HD 980 s that both operate in the long wave infrared spectral range (LWIR) covering 7.5 to 14 μm. According to the manufacturer the cameras measure with an absolute accuracy of $\pm$1.5C and a resolution of 0.05C. The measurements were either conducted with a 15 mm or a 30 mm lens. With the used IRT cameras and lenses the pixel size of the footprint is approximately 1 m with the old camera and 0.5 m with the newer model. Since cold and dry atmospheric (determined by an automatic weather station close by) and snow conditions prevailed during ~~all conducted avalanche experiments~~ avalanche experiments #1 and #2 an emissivity value of 1 has been chosen for all post-processing operations.

Even though in our study we use the IRT measurements mainly in a qualitative way, a basic verification was conducted. ~~The snow surface temperatures recorded~~

The surface temperatures measured with the IRT camera (~~solid~~ lines in Fig. 4) were compared to ~~manually measured snow surface temperatures (dots~~ the corresponding manually measured temperatures (diamonds in Fig. 4) at the ~~corresponding~~ snow profile locations (Fig. 2). The ~~snow surface temperatures of the release ($IRT_{release}$) was compared to~~ release sliding surface temperature measured with the IRT camera ($IRT_{release\_sliding}$, blue continuous line in Fig. 4) has been compared with the corresponding layer in the ~~snow profile in the undisturbed snow ($T\_P_{release}$~~ manual profile performed close to the release zone ($T\_P_{release\_sliding}$, blue full diamond at 0 min)~~and measured surface temperatures with a digital thermometer ($T\_P_{release}$ at 45 min) . The same was conducted for~~ . The avalanche sliding surface temperature measured with the IRT camera in the upper part of the track ($IRT_{track\_sliding}$, orange continuous line in Fig. 4) has been compared with the corresponding layer in the manual profile performed close to the flowing zone ($T\_P_{track\_sliding}$, orange full diamond). Further, the surface temperature ~~along the erosion layer in the avalanche path (T_P_{track}) . Both measurements~~ of the undisturbed snow close to the snow profile location in the release and in the track ($IRT_{release\_undisturbed}$ and $IRT_{track\_undisturbed}$, blue and orange dashed lines) have been compared to snow surface temperature measurements at the profiles

($T\_P_{release\_undisturbed}$ and $T\_P_{track\_undisturbed}$, empty diamonds). Measurements are in fairly good agreement with an absolute difference of about ~~$\pm 1°C$.~~ $\pm 1.5°C$ (except for $T\_P_{track\_sliding}$). This accuracy suggests that the data cannot be used to quantify precise absolute temperature values, but to get an order of magnitude between relative differences.

2.5 Terrestrial laser scan (TLS) and mass balance

A terrestrial laser scanner (Riegl LPM-321) was operated from the Flueelapass road (Fig. 2) to acquire digital surface models before and after the avalanche releases. ~~The~~ These measurements facilitated the calculation of the release~~and erosion depths~~, entrainment and deposition area. Furthermore, the difference between the two laser scans allowed to calculate the spatially averaged release and erosion depth along the path. The combination of area, release/erosion depth and depth-averaged snow density from the manually created snow profiles (Section 2.2) allowed to calculate the corresponding mass. Adding release and entrained mass results in the deposited mass. This procedure is common practice and was applied in multiple other studies (Sovilla et al., 2007, 2010; Steinkogler et al., 2014b) .

A complete set of terrestrial laser scans is available for avalanche #3 only. For avalanche #2 the scan before the avalanche is only available for the release zone (Fig. 2). No information from terrestrial laser scanning was available for avalanche #1. Avalanche boundaries and field measurement locations were recorded by GPS allowing spatial referencing with the TLS data. ~~The underlying (summer)~~ A summer digital elevation model ~~was available~~ (DEM) was available from an airborne digital photogrammetry campaign (Bühler et al., 2015) with 1 m spatial resolution. It was mainly used to georeference our data and allow consequent processing in a GIS system. Furthermore, the summer DEM allowed to determine the topography below the lateral transects in the avalanche deposits (Section 2.3).

3 Investigated avalanches

This section summarizes the key characteristics and available data (Table 1) of the avalanches. All avalanches were released after a snow storm by triggering the cornices at the ridge at 2900 m a.s.l. with explosives. Therefore, most of the released snow was new snow. Yet, two of the avalanches, avalanche #2 and #3 (Fig. 1b and c), entrained significant amounts of snow from deeper layers due to a secondary release in a deeper weak layer, below the rock face. Since the main mass contribution can be assumed to be defined by the secondary releases and the entrainment along the path, we focused our investigations on these snow masses. Mass contributions by the cornices are usually relatively small compared to entrained snow on the open slope below.

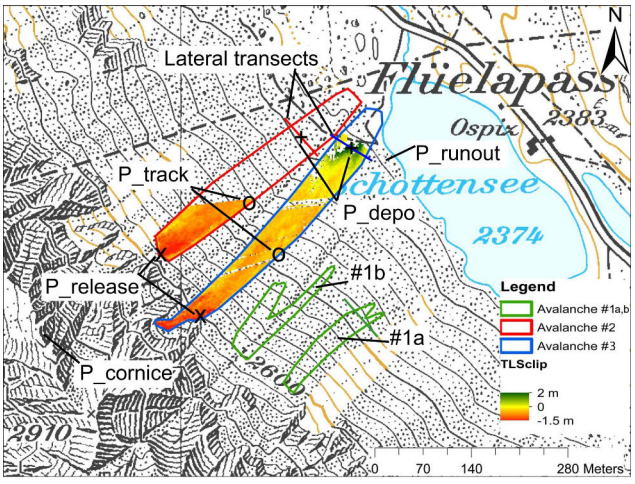

Figure 2. Flueelapass field site close to Davos (Switzerland). Outlines of avalanche #1a and #1b (green), #2 (red) and #3 (blue). The colorbar shows differences between terrestrial laser scans before and after the individual avalanches. $P_{release}$ and P_{track} indicate locations of snow profile in the release and along the path, respectively. Red and blue lines indicate positions of lateral investigations and deposition snow profile P_{depo}.

Furthermore, entrainment of snow in the gullies of the rock face is not assumed to contribute a significant amount since regularly occurring (small) avalanches and slides continuously erode the snow cover. In this study we use the word release to refer to profile locations at the secondary release below the rock face (Fig. 2).

Table 1. Summary of measurements for the investigated avalanches. * indicate that erosion and deposition depths were too small. Growth Index I_g is defined as $I_g = m_e/m_r$.

Avalanche	**#1a**	**#2**	**#3**
Date	23 Jan. 2013	05 Feb. 2013	31 Jan. 2014
IRT camera model	hr 384 sl	hr 384 sl	HD 980 s
Terrestrial laser scan	no	partly	yes
Snow profiles lateral	-*	yes	yes
Snow profiles track	-*	yes	yes
IRT video	yes	yes	no
IRT pictures	yes	yes	yes
Released mass m_r (t)	-	502	818
Entrained mass m_e (t)	-	1857	1302
Deposited mass m_d (t)	-	2359	2120
Growth Index I_g	-	3.7	1.6

Avalanche #1a and #1b (23 January 2013):
In the days previous to the avalanche experiment 10 cm of new snow were recorded and snow drift accumula-

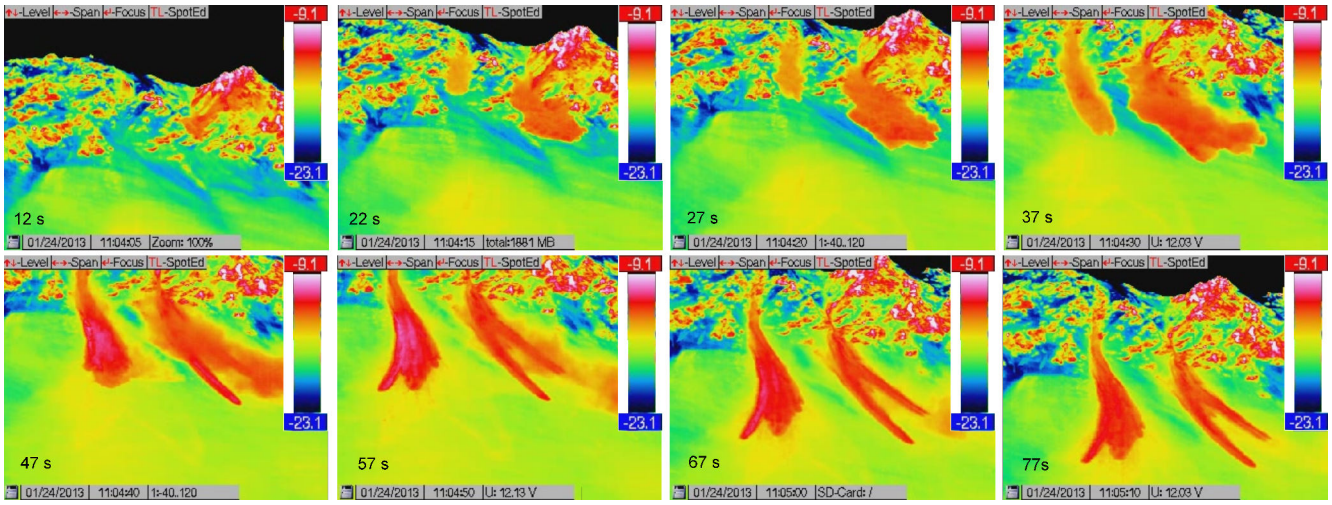

Figure 3. Screenshot of IRT camera videos for avalanche #1a and #1b. The first picture was taken 12 s after the avalanche released.

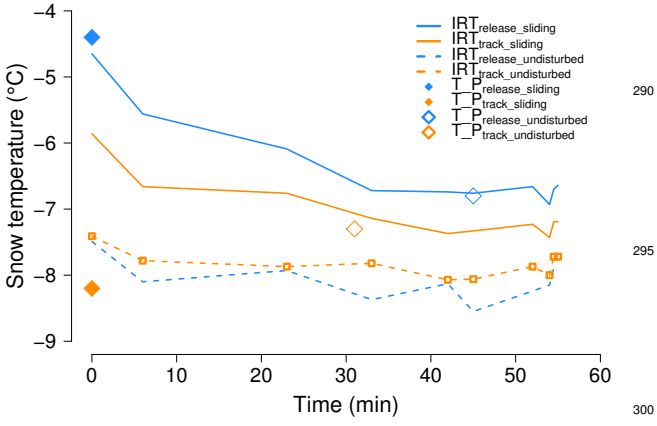

Figure 4. Temporal evolution and comparison of snow temperatures of avalanche #2 using ~~a~~ an IRT camera and manually measured data. Solid lines represent ~~regular~~ IRT measurements in the release (~~$IRT_{release}$~~ blue line) ~~, the deposition area~~ and track (~~IRT_{depo}~~ orange line) ~~and~~ sliding surfaces. Dashed lines represent IRT measurements performed in the undisturbed snow cover close to the release (~~IRT_{snow}~~ blue) ~~which~~ and close to the avalanche path (orange). Small dots on the orange dashed line correspond to the time resolution of all IRT measurements. Data from IRT are compared ~~to~~ with manual measurements performed at the ~~profile locations~~ corresponding layer (~~$T\_P_{release}$~~ filled diamonds) and ~~T_P_{track}~~ at the snow surface (empty diamonds) at the closest snow profile.

tions formed due to strong southerly winds. The national avalanche bulletin reported a moderate avalanche danger (level 2) and identified the fresh snow drift accumulations as the main danger. During the experiment clear sky conditions prevailed and the automatic weather station (AWS) at the Flueelapass (FLU2) measured an air temperature of -10C. Multiple charges were exploded on the ridge to the lookers-left (South) of the summit resulting in two independent small powder avalanches which followed the gullies (Fig. 1a and Fig. 3). Due to the relatively small release mass and no significant entrainment both avalanches, #1a and #1b, stopped half way down the open slope. Even though the avalanches were small and a full data set of field measurements is not available, they are retained in this study since they provide good quality IRT data (Fig. 3). We excluded the snow profile measurements from the analysis since the erosion and deposition depths were very small, around 0.1 m, and the manual measurements were conducted more than 1 hour after the release. The deposition zone was not accessible before due to safety reasons. The TLS could not be completed due to technical problems.

Avalanche #2 (~~25~~ 5 February 2013):
20 cm of fresh snow that covered older snow drift accumulations resulted in a considerable (level 3) avalanche danger. Furthermore, the bulletin noted that avalanches in isolated cases could be released deeper within the snowpack. The AWS at Flueelapass measured -12C and a partly cloudy sky prevailed during the experiment.

Explosions along the ridge and to the lookers-left (South) side of the summit only produced small avalanches that stopped shortly below the rock face. A single explosion that triggered the cornice to the right side of the summit caused another small powder avalanche that followed the gully and triggered a secondary release at the start of the open slope (Fig. 1b). Even though the avalanche almost stopped after entering the open slope, the additional mass which was entrained resulted in an re-acceleration resulting in a long running medium-sized avalanche (deposition mass 2357 t) which only stopped in the flat part close to the lake. Average snow density of the release was 170 $kg\ m^{-3}$ and 210 $kg\ m^{-3}$ for the entrained snow. No full TLS was

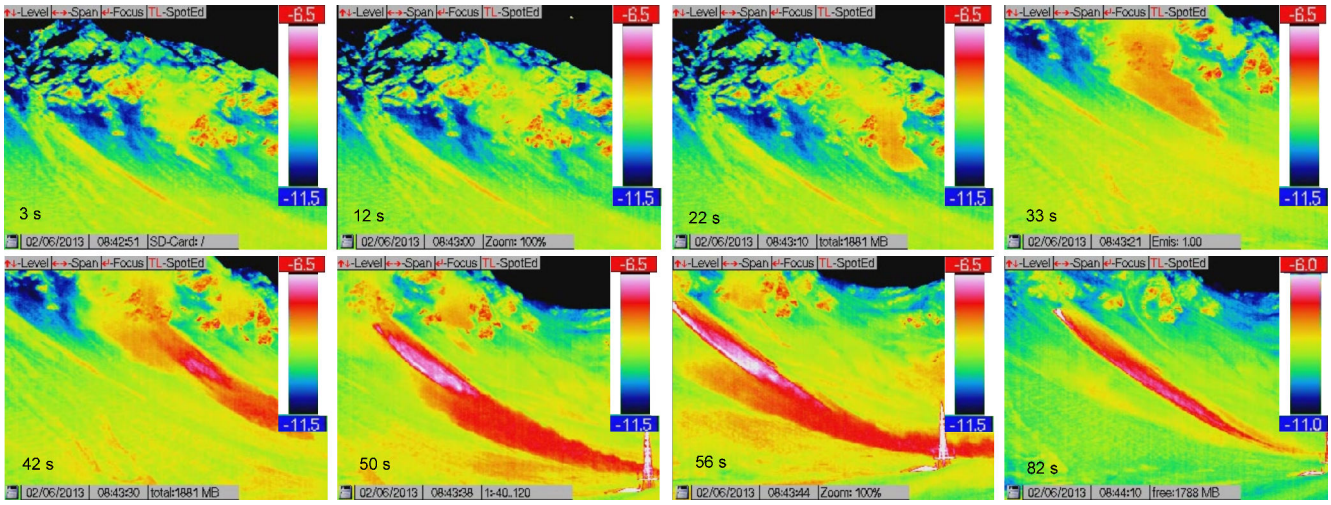

Figure 5. Screenshot of IRT camera videos for avalanche #2. The first picture was taken 3 s after the avalanche released. Note that the temperature scale was changed by 0.5C for the last shown image (82 s).

available before the avalanche release. Nevertheless, in-field observations showed the surface before the release and the entrainment depth to be rather homogenous along the slope which allowed to extrapolate the upper entrainment area, in combination with the envelope of the avalanche acquired with GPS, and thus to calculate the entire entrained mass.

Avalanche #3 (31 January 2014):
Multiple consecutive smaller snowfalls and strong southerly winds created snow accumulations close to ridges. The national avalanche bulletin issued a considerable (level 3) danger level and that the weak old snowpack could cause avalanches to be released in near-ground layers. Moderate winds with gusts up to 60 km/h from the South and cloudy to overcast conditions prevailed during the experiment. The automatic weather station FLU2 recorded -6C with steadily increasing temperatures during the experiment.

Two small spontaneous avalanches already released before the experiment. Initial bombing of the main gully and to the lookers-left (South) of the summit did not produce any significant avalanches. Yet, the bombing of the cornice to the lookers-right (North) of the summit resulted in a small powder avalanche which triggered a second slide at the lower end of the rock face (similar to avalanche #2). Consequently a significant amount of snow was eroded and resulted in a medium-sized avalanche (deposition mass 2120 t) that stopped in the flat run out zone (Fig. 1c). The secondary release nearly entrained all layers to the bottom of the snowpack (1.6 m). Average snow density of the release was 270 $kg\ m^{-3}$ and 310 $kg\ m^{-3}$ for the entrained snow. For avalanche #3 snow temperature measurements were also available for the cornice at the ridge.

4 Results

Based on these measurements we present observed temperature distributions during the avalanche motion as well as at the surface and inside the deposition zone (Section 4.1). In a second step potential sources of thermal energy are identified and quantified (Section 4.2).

4.1 Temperature distribution

4.1.1 Avalanches in motion

The use of the IRT camera gave very interesting qualitative insights into the temperature behavior of a moving avalanche (Fig. 3 and 5). Especially plume formation, entrainment of warmer snow and the stopping of the avalanche as the powder cloud starved and drifted aside could be very well observed. (See supplementary material for the videos).

Even though avalanche #1a was small, a significant powder cloud developed shortly after the release (Fig. 3). After the avalanche entered the open slope (37 s), plume formation stopped, accompanied by a visible decrease in velocity, and the powder cloud drifted to the up-hill looking right side (47 s) due to the prevailing wind, revealing the until then obscured dense core (57 s). After that a rapid cooling of the surface of the dense core could be observed (from pink colors at 57 s to orange at 77 s).

The IRT video of avalanche #2 (Fig. 5) is of special interest since a distinct acceleration of the avalanche can be observed as it approaches the open slope below the rock face (33 s). This can be explained by the entrainment of mass of the secondary release (42 s). The powder cloud shows higher temperatures than during the first phase (50 s) and the eroded surface becomes visible after the powder cloud drifts aside (56 - 82 s). Even though continuous IRT images were acquired

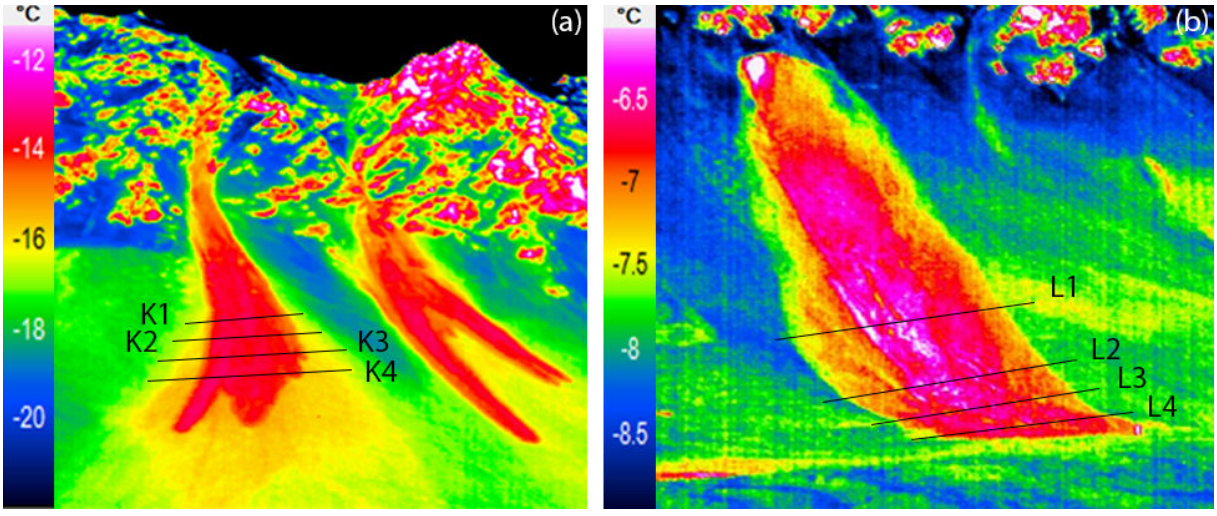

Figure 6. IRT camera images for avalanches (a) #1a and #1b and (b) #2. Note the different temperature scales amongst the avalanches. Black lines indicate positions of lateral snow temperature transects.

during and after avalanche #3 this data could not be used in this study as clouds were preventing an undisturbed view on the slope most of the time.

4.1.2 Surface temperature distribution

The IRT camera images acquired shortly after the avalanches stopped (Fig. 6) allowed to identify exposed deep, and thus warmer, layers in the release and along the path as well as in the deposited snow. In Fig. 6b the secondary release, below the steep rock part, showed a much deeper erosion in the, looking up-hill, left corner. In the lower part of the track erosion was spatially rather homogenous for all avalanches.

Lateral IRT surface temperature transects in the deposition area of avalanche #1 and #2 (black lines in Fig. 6) revealed that the warmest part of the avalanche is located in the center and therefore in its dense core (Fig. 7a and c). In both cases a distinct difference in surface temperature ~~of multiple degree Celsius~~ between undisturbed snow cover and warmer core of the avalanche is evident. Figure 7b shows lateral profiles (L1 and L2 in Fig. 6b) along the path of the avalanche. These coincide with in-field measurements of the undisturbed snow cover, a thin-deposit layer that formed at the lookers-left (South) side of avalanche #2 and the dense core.

4.1.3 Internal temperature distribution of deposits

The observed maximum temperatures in the dense core area did not only exist on the surface in lateral extension (Fig. 7) but also vertically in the deposits. This could be measured for both avalanches for which lateral investigations were conducted. Figure 8 shows the lateral temperature measurements conducted in the deposition zone of avalanche #2 and #3. Measurement P_{depo}, corresponding to 0 m, was located

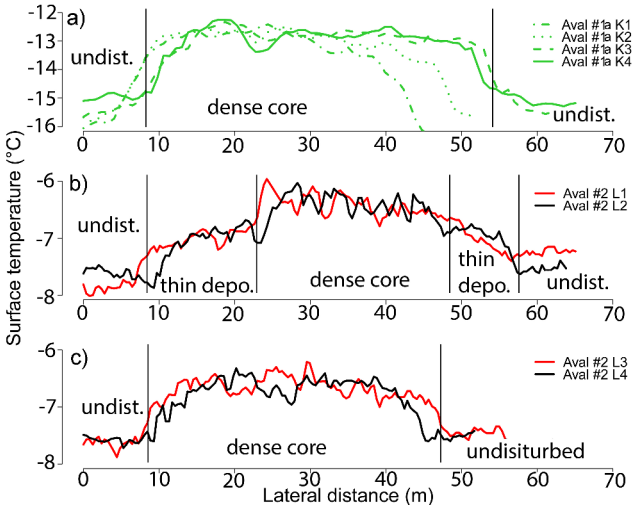

Figure 7. Snow surface temperatures acquired with IRT along lateral transects for avalanche #1 (a) and in the path (b) and the deposition area (c) of avalanche #2. Extent of undisturbed snow cover, thin-deposit and dense core are indicated. The lateral distance was calculated by referencing and scaling with the measured width of the avalanche.

in the middle of the deposition and marked the position of the full snow profile in the deposits (Fig. 2). Temperature measurement locations R and L were leading laterally from the center to the, looking uphill, right and left side of the avalanche deposits. Furthermore, the top of the avalanche deposits (solid line), the bottom of the deposits (dashed line) and the terrain (pointed line) are indicated. For better distinction the area of the undisturbed snow cover is additionally indicated by softened colors. Even though the transect shown in Fig. 8a only represents one half of the avalanche

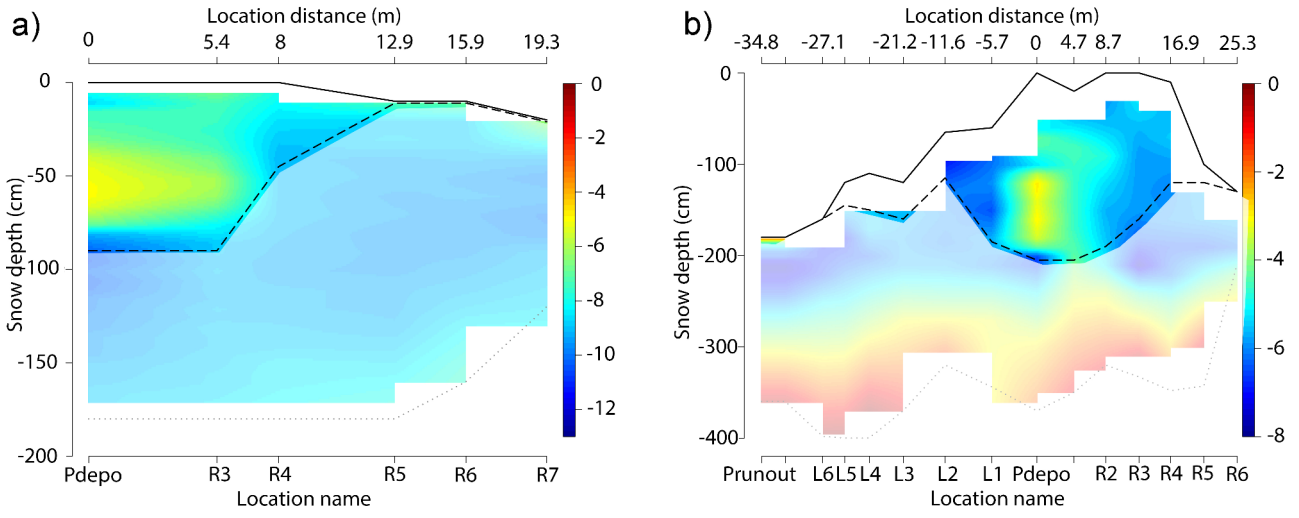

Figure 8. Lateral snow temperature profiles in the avalanche deposits of (a) avalanche #2 and (b) avalanche #3. P_{depo} and 0 m indicate the center of deposits and the index L and R represent left and right, looking uphill, measurement locations towards the lateral sides of the avalanches. Lines indicate the top of the avalanche deposit or snow cover (solid), bottom of avalanche deposit (dashed) and bottom of snow cover (pointed). Colors of undisturbed snow cover were softened for better distinction with avalanche deposits.

deposits from avalanche #2, the extent of the dense core (area between solid and dashed line) could clearly be observed in the measured snow temperature. Similar measurements were recorded for avalanche #3 where again the highest temperatures were recorded in the center of the deposits (Fig. 8b) with decreasing values towards the side of the deposits.

4.2 Thermal energy sources

To explain the observed increase in snow temperatures in the deposits of the investigated avalanches and to assign an order of magnitude estimation of the sources of thermal energy, we look at two important sources of energy, namely (i) friction and (ii) warming due to entrainment of snow. Other potential sources of thermal energy, e.g. entrainment of air or adiabatic warming, were not further considered since an order of magnitude estimation revealed that their influence on the temperature of the dense core is negligibly small (not shown).

Figure 9 shows snow temperature profiles in the center of the deposition zone T_P_{depo} (~~solid~~ violet line) and compares them to measurements conducted in the release zone $T\_P_{release}$ (blue line), along the path in the undisturbed snow T_P_{track} (orange) and the undisturbed snow cover in the run out zone T_P_{runout} (gray). Depth-averaging the deposition profile (solid violet line in Fig. 9) yielded a snow temperature of -6.8C for avalanche #2 and -4.1C for avalanche #3 ($\overline{T\_P}_{depo}$ in Table 2). ~~Temperature~~ For T_P_{depo} the temperature values from the upper and lowermost layers (0.2 m thick) were excluded from the calculations because of adaption of the temperature with the surrounding air and undisturbed snow cover (gray areas in Fig. 9). Since $\overline{T\_P}_{depo}$ only represents the relatively warm core of the deposits we additionally calculated the mean of the lateral temperature profiles (Fig. 8) resulting in a mean temperature of the deposits $\overline{T}_{depo\_lateral}$ of -7.4C and -4.8C for avalanche #2 and #3, respectively.

Comparing the mean temperature of the deposits $\overline{T}_{depo\_lateral}$ with $\overline{T\_P}_{release}$ reveals that a significant warming took place. This resulted in a difference in snow temperature between released and deposited snow of ΔT 1.2C and 1.5C for avalanche #2 and #3, respectively (Table 2).

4.2.1 Friction

The increase in temperature due to friction was calculated by assuming that all potential energy is transformed to heat. This means that the increase in temperature is only given by the drop height of the average avalanche mass:

$$m\ c_p\ \Delta T = m\ g \Delta h, \tag{1}$$

where m is the mass undergoing the change in potential energy, c_p is the specific heat capacity of snow (2116 $J\ kg^{-1}\ K^{-1}$), ~~$\Delta T_{friction}$~~ ΔT is the change in snow temperature, g is the gravitational acceleration (9.81 $m\ s^{-2}$) and Δh is the difference in elevation. Thus, ~~ΔT~~ the temperature increase due to friction $\Delta T_{friction}$ is given by

$$\Delta T_{friction} = \frac{g \Delta h}{c_p}. \tag{2}$$

This equation has general validity for any (incremental or finite) mass, in which potential energy is converted to heat. This is regardless of whether this mass is added to the

avalanche by entrainment or whether it belongs to the initial release mass as long as Δh is the effective height drop of this mass. Calculating for an elevation drop of 300 m, corresponding to the slope below the rock face until the run out zone, we obtain an increase in temperature due to friction of approximately ~~1.5~~1.4C.

The calculated $\Delta T_{friction}$ can be seen as an upper limit in our order of magnitude estimation since in nature not all mass is released and entrained at the maximum elevation. Furthermore, lateral temperature gradients in the deposition area are not taken into account. In practice avalanches entrain large portions of mass along the avalanche path. In many cases the entrained mass, m_e, is significantly larger than the released mass, m_r. This is also the case for the investigated avalanches which are characterized by a growth index of 3.7 and 1.6 for avalanche #2 and #3, respectively. If one further assumes that entrainment is happening uniformly along the path and that the vertical extension of the release area is small compared to the total path vertical drop, the entrained mass only experiences on average half the height drop of the released mass: $\Delta h_e = 0.5 \Delta h_r$. The effective Δh for Eq. 2 can then be calculated:

$$\Delta h = \frac{\Delta h_r \ (m_r + 0.5 m_e)}{m_r + m_e}. \quad (3)$$

For avalanche #2 and #3 this corresponds to a warming due to friction, $\Delta T_{friction}$, of ~~0.8 and 0.9~~ 0.84 and 0.96 C, respectively.

4.2.2 Entrainment at a different temperature

The above development assumes that there is no difference between initial snow temperatures of the released and entrained snow. The snow profiles (see locations in Fig. 2) enabled a quantification of the properties of the released and entrained snow showing some difference as discussed above. Assuming that the ~~entrained snow is~~ snow that is entrained along the track is completely mixed with the released snow in the deposition zone ~~and that $\Delta T_{rel-ent}$ is this~~ results in the mean temperature difference between ~~mass released and entrained , this~~ entrained ($\overline{T\_P}_{track}$) and released snow ($\overline{T\_P}_{release}$). This difference leads to the following difference in temperature at the deposited snow mass:

$$\Delta T_{entrainment} = \frac{(\overline{T\_P}_{track} - \overline{T\_P}_{release})\ m_e}{m_r + m_e}. \quad (4)$$

This results in a change in temperature due to entrainment $\Delta T_{entrainment}$ of -0.08C and 0.3C for avalanche #2 and #3, respectively. Since we assume that the heating due to friction is independent of the initial snow temperature either from release or entrainment, at least as long as the snow remains dry during warming, the temperature change due to a different snow temperature of the entrained snow can simply be added to the one from friction in Eq. 2. ~~This results in a warming due to entrainment $\Delta T_{entrainment}$ of 0.08C and 0.3C for avalanche 2 and 3, respectively.~~

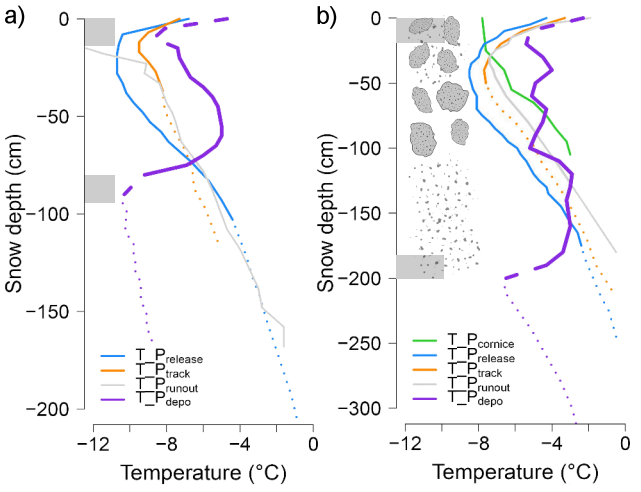

Figure 9. Snow temperature measurements conducted in the undisturbed snow cover close to the release zone ($T\_P_{release}$), along the path ~~in the undisturbed snow~~ (T_P_{track}) ~~,~~ and in the ~~undisturbed snow cover in the~~ run out zone (T_P_{runout}) ~~and~~ as well as in the deposition zone (T_P_{depo}) of (a) avalanche #2 and (b) avalanche #3. Release, entrainment and deposition depths are indicated by solid lines whereas the undisturbed snow cover is represented by pointed lines. Gray areas and dashed lines indicate parts of the temperature profiles in the deposits (T_P_{depo}) that were neglected in the calculations because of expected changes in temperature over time due to the boundary conditions of the surface and the undisturbed snow cover. Composition of deposits (granules and fine grains) are indicated for avalanche #~~2~~3.

Table 2. Depth averaged temperatures of release ($\overline{T\_P}_{release}$), track ($\overline{T\_P}_{track}$) and deposition profile ($\overline{T\_P}_{depo}$) with the corresponding release and erosion depths (in brackets). $\overline{T}_{depo\_lateral}$ represents the mean of the lateral temperature measurements in the deposition. ΔT is the difference between $\overline{T}_{depo\_lateral}$ and $\overline{T\_P}_{release}$. $\Delta T_{friction}$ and $\Delta T_{entrainment}$ are the individual contributions to ΔT.

Avalanche	#2	#3
$\overline{T\_P}_{release}$	-8.6C (1.03 m)	-6.3C (1.75 m)
$\overline{T\_P}_{track}$	-8.7C (0.37 m)	-5.8C (0.3 m)
$\overline{T\_P}_{depo}$	-6.8C (0.9 m)	-4.1C (1.95 m)
$\overline{T}_{depo\_lateral}$	-7.4C	-4.8C
ΔT	1.2C	1.5C
$\Delta T_{friction}$	~~0.8~~0.84C	~~0.9~~0.96C
$\Delta T_{entrainment}$	~~0.08~~-0.08C	0.3C

5 Discussion

It has been noted in other studies (Vera et al., 2012) that potential sources of thermal energy in snow avalanches are friction processes or entrainment of snow with differing temperatures. The investigated avalanches in this study indicate that the thermal energy increase was mainly defined by frictional heating, which in turn depends only on the ~~elevation drop~~effective elevation drop (Section 4.2.1). Yet, it is well known that avalanches can significantly increase their mass along the path via entrainment (Sovilla et al., 2006). Also for the investigated avalanches the growth index were I_g of 3.7 and 1.6 for avalanche #2 and #3, respectively. Therefore, the calculated (maximum) value of ~~0.5~~approximately 0.46C per 100 altitudinal meters (Eq. 2) has to be adapted to consider the actual mass that enters the avalanche at a certain point along the track (Section 4.2). For dry and cold snow avalanches far away from the melting point, the warming due to friction alone is not expected to have a substantial influence on flow dynamics. Yet, if the overall avalanche temperature is already close to the critical temperature threshold of -1C (Steinkogler et al., 2014a) the warming by frictional processes can cause drastic changes of the granular structure inside the avalanche and consequently affect flow behavior.

Contrary, the warming due to entrainment varied for the individual avalanches. These variations depend on the temperature of the snow and the erosion depth as shown in the profiles along the avalanche track (Fig. 9) and the IRT pictures (Fig. 6). Typically, the alpine snow cover shows a positive temperature gradient towards the ground (Armstrong and Brun, 2008). Except for areas with permanent permafrost, the temperature at the soil-snow interface can be assumed to be approximately 0C if there has been a significant snow cover for several weeks. Consequently, the erosion of deeper snow layers leads to warmer snow temperatures (Fig. 9). Also changes of snow temperature due to elevation gradients have been proven to be quite variable and directly influence flow dynamics (Steinkogler et al., 2014b). As in the case of avalanche #2 even a cooling of an avalanche is possible when the avalanche released into deep layers but entrained only superficial (cold) layers of snow, e.g. blue and orange lines in Fig. 9. Overall, the contribution of the temperature of the entrained snow to the ~~warming~~ temperature change was smaller than by friction for the investigated avalanches (Table 2).

Our temperature measurements on the surface (Fig. 7) and in depth (Fig. 8) of the deposit indicate that the highest temperatures are located in the dense core of the avalanche. The interface between the bottom of the avalanche deposits and the subjacent undisturbed snow cover featured a very clear and sharp transition (violet lines in Fig. 9). The shape of the temperature curve indicates the warmest temperatures in the lower parts of the deposits profile (-0.4 to -0.8 m and -1.2 to -1.9 m for avalanches #2 and #3, respectively) and close to the sliding surface. This would support the expectation of the most pronounced friction at the bottom of the flow, typical for this kind of avalanche. Unfortunately, a cooling of the lowest deposition layers to the temperature of the subjacent undisturbed snow cover has to be expected and thus prevents a definite conclusion on this observation. Also, whether the small temperature variations in the upper part of the deposition profile between 0 and -1 m of avalanche #3 (violet line in Fig. 9) are a result of a mixture of broken parts of the eroded snow cover, with varying temperatures, and formed granules could not be fully answered. Yet, granules embedded in fine grained snow were still clearly observable in this area of the deposition.

It is without question that reaching the deposits after an avalanche release to measure the snow surface temperature with traditional methods, e.g. thermometers, takes too long and the surface as well as the upper most layers would have changed their temperature already. It could be observed in the video of avalanche #1 (see supplementary material) that right after the dense core stopped it started to cool. In all those cases for which a real-time measurement is necessary IRT technology provides a valuable addition to traditional measurements. Even though in our study we only applied the IRT camera in a qualitative way, the presented basic verification (Fig. 4) with manually measured snow surface temperatures showed a fairly good agreement with an accuracy of about $\pm$1.5C. Although further investigations are necessary to define whether absolute values of surface temperature can be acquired without significant uncertainties, the relative accuracy of the IRT cameras are usually high, around 0.05C in our case as specified by the manufacturer. This facilitates to track relative changes in temperatures even if the absolute value might not be accurate.

Recently IRT was mainly tested and evaluated for snow profile applications at short distances (Schirmer and Jamieson, 2014). Dozier and Warren (1982) investigated the effect of viewing angle on the infrared brightness temperature of snow and found differences of up to 3C. Similar values have been found by Hori et al. (2013), yet they concluded that for viewing angles less than 40 from the nadir the error in temperature is less than -0.8C. The effect of moisture has been studied extensively (Wu et al., 2009, and references therein), basically concluding that the presence of water causes a strong absorbance and consequently a decrease in reflectance in the near-infrared spectra of soils. In general, low signal attenuation can be expected for (peak) winter month atmospheres, especially for clear sky conditions, due to relatively low humidity levels. An effect that still illustrates challenges for the interpretation of IRT images is due to the roughness of the investigated surface (Wu et al., 2009). In most studies the assumption that the scene elements are isothermal, smooth and homogenous is used (Danilina et al., 2006). Consequently supposing that the object of interest is Lambertian, i.e. behaves as a perfect diffuser and emits and reflects radiation isotropically. Mushkin et al. (2007) observed that the effective emissivity spectra of rough surfaces are different from those of perfectly smooth surfaces of the

same composition due to multiple scattering among roughness elements. Yet, they only found an up to 3% reduction in the spectral contrast due to sub-pixel surface roughness variations. This might also be the case for situations similar to the presented application as size of the granules, i.e. the sub pixel structures, are much smaller than the pixel size (0.5 to 1 m).

Also whether the surface temperature, and possibly even the composition, of the aerosol mixture of the powder cloud can be measured is an open question. Visualization of air flows on the qualitative level is common practice for various applications (Narayanan et al., 2003; Carlomagno and Cardone, 2010) and, as presented in this study, provides impressive footage of powder snow avalanches. Usually a tracer is injected into the flow field. In our case the tracer is already present by snow particles of the entrained snow which are transported into the powder cloud. Similar concepts as applied for satellite remote sensing of high-level clouds, such as cirrus (Fu et al., 1998), might be transferable to avalanche powder clouds.

A possible further application of IRT could be the differentiation of flow regimes in the deposition area. As shown earlier the warmest part of an avalanche is located in the dense core, e.g. center (red and pink) of avalanche #2 in Fig. 6b, whereas layers with less mass or where less friction occurred are cooler (yellow and orange areas in Fig. 6b). Especially the lookers-left (South) side thin-deposit area in Fig. 6b might be associated with the deposits of a fluidized layer (Issler et al., 2008). The IRT observations of this thin-deposit area are in agreement with the field observation criteria for fluidized layers as described by Issler et al. (2008): (1) rapid decrease of deposit thickness, (2) snowballs of various sizes embedded in a matrix of compacted fine-grained snow, (3) large snowballs lying on top of the deposit and (4) fewer snowballs per unit area than on the dense deposit.

~~For the investigated avalanche the deposits from the powder cloud~~ The powder clouds of the investigated avalanches (see Fig. 3 and 5 and corresponding videos) had consistently lower temperatures than the warm dense core despite the fact that the powder cloud (at least from one avalanche) traveled as far downhill as the dense core. Two distinct processes may contribute to this fact: (i) A preferential ejection of colder and lighter surface with colder snow while the dense core may have a higher fraction of snow from lower layers in the profile and therefore with a higher temperature. (ii) The particle concentration in the suspension layer is low and therefore molecular dissipation of kinetic energy and exchange of sensible and latent heat happens largely between air and snow and not between snow and snow particles as in the dense core. This leads to a rapid adoption of temperatures close to the air temperature for the suspended snow.

Furthermore, the IRT results can be qualitatively interpreted in a similar way as a laser scan to identify areas where deeper or shallower erosion occurred, e.g. see entrainment by secondary release below the rock face for avalanche #2 (Fig. 6b). For this avalanche we exemplary calculated the release mass solely by using information from the IRT pictures and manually measured snow profiles in the release. Therefore, the IRT picture was georeferenced in a GIS software and shallower and deeper release layers were identified. The (IRT) surface temperature of these layers were combined with the snow height of the corresponding temperature in the conducted snow profile in the release. This resulted in a calculated release mass of 457 t which is similar to the mass measured with the terrestrial laser scan (502 t). This depicts a rough yet quick and efficient method to estimate the release mass of an avalanche. As shown in this study, the release and entrainment depth does not only define the overall mass of snow but equally important its temperature. IRT pictures and videos provide an intuitive and easy way to identify these relevant erosion processes (Fig. 6).

6 Conclusions

We conducted full-scale avalanche experiments at the Flueelapass field site above Davos (Switzerland) to investigate the distribution of snow temperatures in avalanche deposits and identify the sources of thermal energy in dry avalanches. A further goal was to test the usability of infrared radiation thermography (IRT) in this context.

For the investigated similar avalanches the temperature increase due to friction has been shown to dependent on the ~~elevation the~~ effective elevation the mass inside the avalanche dropped. The contribution to the total temperature increase by erosion processes was shown to be quite variable, depending on the release depth and snow temperatures of the entrained snow. The warmest temperatures were observed in the center of the avalanche deposits and thus represented the dense core of the flowing avalanche.

The IRT camera allowed to observe the avalanche phenomenon 'with different eyes' and provides a lot of potential for more detailed research in the field of avalanche dynamics, both quantitative and qualitative. It is still necessary to further verify the measurements and define to which extent absolute snow surface temperatures can be measured. Then, the spatial distribution of surface temperatures can help in the interpolation of profile temperatures measured by hand.

Our results allow for a more comprehensive understanding of snow temperatures in avalanche flow and their consequences on flow regimes. This information can directly be used to verify and enhance the performance of avalanche dynamics models and is thus of great interest for practitioners.

Acknowledgements. Funding for this research has been provided through the Interreg project STRADA and STRADA 2 by the following partners: Amt fuer Wald Graubuenden, Etat du Valais, ARPA Lombardia, ARPA Piemonte, Valle d'Aosta, Regione Lombardia. The authors would like to thank all the people who helped gathering the data during the field experiments and Perry Bartelt

for his valuable input. Thanks to Vali Meier from the SOS Service Jakobshorn (Davos) and his team for the great support.

References

Armstrong, R. L. and Brun, E.: Snow and Climate: Physical Processes, Surface Energy Exchange and Modeling, Cambridge University Press, Cambridge, UK, 222 pp., 2008.

Bartelt, P., Bühler, Y., Buser, O., Christen, M., and Meier, L.: Modeling mass-dependent flow regime transitions to predict the stopping and depositional behavior of snow avalanches, J. Geophys. Res., 117, http://dx.doi.org/10.1029/2010JF001957, 2012.

Bates, B., Ancey, C., and Busson, J.: Visualization of the internal flow properties and the material exchange interface in an entraining viscous Newtonian gravity current, Environmental Fluid Mechanics, 14, 501–518, 2014.

Brenning, A., Gruber, S., and Hoelzle, M.: Sampling and statistical analyses of BTS measurements, Permafrost and Periglacial Processes, 16, 383–393, 2005.

Bühler, Y., Marty, M., Egli, L., Veitinger, J., Jonas, T., Thee, P., and Ginzler, C.: Snow depth mapping in high-alpine catchments using digital photogrammetry, The Cryosphere, 9, 229–243, doi:10.5194/tc-9-229-2015, http://www.the-cryosphere.net/9/229/2015/, 2015.

Carlomagno, G. and Cardone, G.: Infrared thermography for convective heat transfer measurements, Experiments in Fluids, 49, 1187–1218, doi:10.1007/s00348-010-0912-2, http://dx.doi.org/10.1007/s00348-010-0912-2, 2010.

Danilina, I., Mushkin, A., Gillespie, A., O'Neal, M., Pietro, L., and Balick, L.: Roughness effects on sub-pixel radiant temperatures in knetically isothermal surfaces, in: RAQRS II: 2nd International Symposium on Recent Advances in Quantitative Remote Sensing, Torrent (Valencia), Spain, 25-29 September 2006, 2006.

Dozier, J. and Warren, S. G.: Effect of viewing angle on the infrared brightness temperature of snow, Water Resources Research, 18, 1424–1434, doi:10.1029/WR018i005p01424, http://dx.doi.org/10.1029/WR018i005p01424, 1982.

Fierz, C., Armstrong, R., Durand, Y., Etchevers, P., Greene, E., McClung, D., Nishimura, K., Satyawali, P., and Sokratov, S.: The international classification for seasonal snow on the ground, IHP-VII Technical Documents in Hydrology, IACS Contribution N1, UNESCO-IHP, Paris., 83, 2009.

Fu, Q., Yang, P., and Sun, W.: An accurate parameterization of the infrared radiative properties of cirrus clouds for climate models, Journal of climate, 11, 2223–2237, 1998.

Gauer, P., Issler, D., Lied, K., Kristensen, K., and Sandersen, F.: On snow avalanche flow regimes: inferences from observations and measurements, paper presented at International Snow Science Workshop ISSW 2008, Whistler, Canada, pp. 717–723, 2008.

Hori, M., Aoki, T., Tanikawa, T., Hachikubo, A., Sugiura, K., Kuchiki, K., and Niwano, M.: Modeling angular-dependent spectral emissivity of snow and ice in the thermal infrared atmospheric window, Appl. Opt., 52, 7243–7255, doi:10.1364/AO.52.007243, http://ao.osa.org/abstract.cfm?URI=ao-52-30-7243, 2013.

Issler, D., Errera, A., Priano, S., Gubler, H., Teufen, B., and Krummenacher, B.: Inferences on flow mechanisms from snow avalanche deposits, Annals of Glaciology, Vol 49, 2008, 49, 187–192, 2008.

Lewkowicz, A. G. and Ednie, M.: Probability mapping of mountain permafrost using the BTS method, Wolf Creek, Yukon Territory, Canada, Permafrost and Periglacial Processes, 15, 67–80, 2004.

Meola, C. and Carlomagno, G. M.: Recent advances in the use of infrared thermography, Measurement Science and Technology, 15, R27, http://stacks.iop.org/0957-0233/15/i=9/a=R01, 2004.

Mushkin, A., Danilina, I., Gillespie, A. R., Balick, L. K., and McCabe, M. F.: Roughness effects on thermal-infrared emissivities estimated from remotely sensed images, in: Remote Sensing, pp. 67 492V–67 492V, International Society for Optics and Photonics, 2007.

Naaim, M., Durand, Y., Eckert, N., and Chambon, G.: Dense avalanche friction coefficients: influence of physical properties of snow, J. Glaciol., 59, 771–782, doi:10.3189/2013JoG12J205, http://www.ingentaconnect.com/content/igsoc/jog/2013/00000059/00000216/art00015, 2013.

Narayanan, V., Page, R., and Seyed-Yagoobi, J.: Visualization of air flow using infrared thermography, Experiments in fluids, 34, 275–284, 2003.

Schirmer, M. and Jamieson, B.: Limitations of using a thermal imager for snow pit temperatures, The Cryosphere, 8, 387–394, doi:10.5194/tc-8-387-2014, http://www.the-cryosphere.net/8/387/2014/, 2014.

Shea, C. and Jamieson, B.: Some fundamentals of handheld snow surface thermography, Cryosphere, 5, 55–66, doi:10.5194/tc-5-55-2011, 2011.

Shea, C., Jamieson, B., and Birkeland, K. W.: Use of a thermal imager for snow pit temperatures, The Cryosphere, 6, 287–299, doi:10.5194/tc-6-287-2012, http://www.the-cryosphere.net/6/287/2012/, 2012.

Snyder, W. C., Wan, Z., Zhang, Y., and Feng, Y.-Z.: Classification-based emissivity for land surface temperature measurement from space, International Journal of Remote Sensing, 19, 2753–2774, doi:10.1080/014311698214497, http://dx.doi.org/10.1080/014311698214497, 1998.

Sovilla, B., Burlando, P., and Bartelt, P.: Field experiments and numerical modeling of mass entrainment in snow avalanches, Journal of Geophysical Research-earth Surface, 111, doi:10.1029/2005JF000391, 2006.

Sovilla, B., Margreth, S., and Bartelt, P.: On snow entrainment in avalanche dynamics calculations, Cold Regions Science and Technology, 47, 69–79, doi:10.1016/j.coldregions.2006.08.012, 2007.

Sovilla, B., McElwaine, J. N., Schaer, M., and Vallet, J.: Variation of deposition depth with slope angle in snow avalanches: Measurements from Vallee de la Sionne, Journal of Geophysical Research-earth Surface, 115, doi:10.1029/2009JF001390, 2010.

Steinkogler, W., Gaume, J., Löwe, H., Sovilla, B., and Lehning, M.: Granulation of snow: from tumbler experiments to discrete element simulations, Journal of Geophysical Research - Earth Surface , submitted, 2014a.

Steinkogler, W., Sovilla, B., and Lehning, M.: Influence of snow cover properties on avalanche dynamics, Cold Reg. Sci. Technol., 97, 121–131, doi:10.1016/j.coldregions.2013.10.002, http://www.sciencedirect.com/science/article/pii/S0165232X13001535, 2014b.

Vera, C., Feistl, T., Steinkogler, W., Buser, O., and Bartelt, P.: Thermal Temperature in Avalanche Flow, paper presented at Interna-

tional Snow Science Workshop ISSW 2012, Anchorage, Alaska, pp. 32–37, 2012.

Vera Valero, C., Wikstroem Jones, K., Bühler, Y., and Bartelt, P.: Release temperature, snow-cover entrainment and the thermal flow regime of snow avalanches, Journal of Glaciology, 61, 173–184, 2015.

Wu, C.-Y., Jacobson, A. R., Laba, M., and Baveye, P. C.: Accounting for surface roughness effects in the near-infrared reflectance sensing of soils, Geoderma, 152, 171 – 180, doi:http://dx.doi.org/10.1016/j.geoderma.2009.06.002, http://www.sciencedirect.com/science/article/pii/S0016706109001803, 2009.